Research Article

Carbon Particle Size from Galangal Rhizomes as the Sustainable Adsorbent: Synthesis and Mathematical Calculation Analysis in the Adsorption Isotherm Characteristics

Asep Bayu Dani Nandiyanto [1,*] [iD], **Alifiyha Nayla Putri Akbar** [1] [iD], **Shilla Aulia Suhandi** [1] [iD], **Risti Ragadhita** [1] [iD], **Dwi Fitria Al Husaeni** [1] [iD], **Meli Fiandini** [1] [iD], **Abdulkareem Sh. Mahdi Al-Obaidi** [2] [iD], **Herry Saputra** [3] [iD], **Senny Luckyardi** [4] [iD], **Muhammad Aziz** [5] [iD]

[1] Department of Chemical Engineering, Faculty of Technology and Industrial Education, Universitas Pendidikan Indonesia, Bandung, 40154, Indonesia

[2] Department of Mechanical Engineering, School of Computer Science and Engineering, Taylor's University, Selangor, 47500, Malaysia

[3] Information Systems Department, Faculty of Engineering and Computer Science, Universitas Komputer Indonesia, Bandung, 40132, Indonesia

[4] Department of Management, Faculty of Economics, Universitas Komputer Indonesia, Bandung, 40132, Indonesia

[5] Department of Mechanical and Biofunctional Systems, Institute of Industrial Science, The University of Tokyo, Tokyo, 153-8505, Japan

*Corresponding Author: Asep Bayu Dani Nandiyanto, E-mail: nandiyanto@upi.edu

Article Info	Abstract
	This study investigates the impact of carbon particle size derived from Galangal Rhizomes on adsorption isotherm characteristics, aiming to establish its effectiveness as an adsorbent. Galangal Rhizomes were selected due to their rich carbon compounds, including cellulose, hemicellulose, lignin, starch, pectin, and fiber, making them ideal for carbon-based adsorbents. The carbonization process involved subjecting Galangal Rhizomes to 250°C for 9 hours, then milling and sieving to obtain specific particle sizes (500, 1000, and 2000 µm). Characterization was done using digital microscopy and Fourier-transform infrared spectroscopy. Batch adsorption experiments were conducted using a curcumin solution as the model adsorbate, comparing results with ten standard isotherm models. Findings revealed that small carbon particles (500 µm) underwent monolayer adsorption, while large particles (1000 and 2000 µm) exhibited multilayer adsorption. The study concluded that Galangal Rhizomes-derived carbon particles are effective for colour waste cleanup, providing a natural, sustainable, and environmentally friendly solution aligned with sustainable development goals (SDGs).

1. Introduction

Adsorption is the physical absorption of molecules of a substance that were previously in solution

onto the surface of an adsorbent [1]. The specification between the adsorbent and substance being adsorbed (adsorbate) determines adsorption. Adsorption can occur physically (when Van der Walls force exists) or chemically (chemisorption). The specification between the adsorbent and adsorbate refers to the physical and chemical properties influencing their interaction during adsorption. Adsorbent properties like surface area, pore size, and surface chemistry affect its ability to attract and hold onto adsorbate molecules. Adsorbate properties like molecular size, shape, polarity, and solubility also play a role in determining adsorption behaviour. Proper consideration of these specifications is important in designing and selecting effective adsorption systems for various applications like environmental remediation and water treatment [2-6]. Adsorption can be carried out using porous carbon. Because of its large surface area and high electrostatic charge on its surface, porous carbon is one of the most unique and interesting materials [7]. Porous carbons are carbon materials with interconnected pores and voids throughout their structure. These pores can range in size from nanometers to micrometres and are typically formed through a combination of templating, activation, and carbonization processes. Porous carbons' high surface area and porosity make them useful in various applications, including gas separation, water purification, energy storage, and catalysis [6].

Carbon is an element that readily combines with various substances to form thousands of organic compounds, composites, and minerals. Synthetic compounds are found in 90% of carbon, and the remaining 10% is present in every process of molecular transformation of living creatures, such as plants, animals, fungi, and microorganisms [8]. Many studies have proven that synthetic carbon can be made from organic materials such as leaves, fruit peels, seeds, and more (see Table 1). Thus, using natural resources as a synthetic carbon-based material has many advantages, such as reducing air, water, and soil pollution because it uses natural materials with environmentally friendly technology [9]. Natural materials or waste can be cheap adsorbents [10].

Using natural resources to make synthetic carbon materials can offer several advantages, including:

1. Sustainability: Natural resources are renewable and can be replenished over time, which means that the production of synthetic carbon materials can be sustainable if appropriately managed. This can help to reduce the environmental impact of the manufacturing process.

2. Cost-effective: Natural resources are often abundant and readily available, making them a cost-effective option for producing synthetic carbon materials.

3. Tailor ability: Natural resources can be processed and modified to produce carbon materials with specific properties such as pore size, surface area, and chemical reactivity. This allows for the customization of synthetic carbon materials for specific applications.

4. Reduced environmental impact: Natural resources can be used to make synthetic carbon materials with a lower environmental impact than other materials, such as plastics or metals. For example, carbon materials can be used instead of plastic in some applications, reducing plastic waste and pollution.

Using natural resources to make synthetic carbon materials can provide a more sustainable and environmentally friendly option for producing materials with tailored properties for various applications. Indeed, this supports the current issues in the SDGs.

Table 1. Previous research on adsorbents

No	Waste Sources	Adsorbent types	Results	Ref
1	Coconut shell	Carbon	The highest adsorption efficiency was 83.57% after 50% KOH activation. The higher the KOH concentration, the more efficient Cu metal absorption will be until the activated carbon pores reach saturation at 60% KOH concentration. Beyond the 60% KOH concentration, the efficiency of Cu metal absorption decreased due to the blockage of the activated carbon pores by KOH particles. The results demonstrate the significance of optimizing the activation process to achieve a given adsorbate's highest possible adsorption efficiency.	[11]
2	Banana peel	Carbon	The low-cost banana peel carbon (ABPC) adsorbent was used to remove Rhodamine B (RHB) from the aqueous media. In both acidic and basic conditions, the synthesized ABPC effectively removes RHB. The findings indicate that data adjustment and model parameter estimation can be accomplished using the Freundlich and Langmuir models. Furthermore, this research determined that the pseudo-second-order kinetic model (with $R^2>0.99$) provided the best fit for RHB adsorption on ABPC. An examination of intra-particle models suggests that pore diffusion did not solely control the rate. Additionally, the adsorption process demonstrates a preference for exothermic behaviour when the enthalpy change falls within the negative range at temperatures between 40°C and 70°C.	[12]
3	Teak leaves	Carbon	Adsorption is achieved by blending activated carbon derived from teak leaves with used cooking oil for three hours and then by analyzing the residual FFA levels. The experimentation reveals that as the concentration of NaOH increases, so does the quantity of absorbed FFA. The optimal adsorption of FFA is observed when activated carbon sourced from teak leaves is activated with a 20% NaOH solution.	[13]
4	Tea dregs	Carbon	Adsorbents were produced by synthesizing chitosan and activated carbon from tea dregs. Characterization outcomes indicate that activated carbon effectively captured 78.09% of the carbon content present in a 1.02 mg/L Pb solution. Consequently, the introduction of 1.4 grams of activated carbon derived from tea waste successfully lowered the concentration of Pb heavy metal, aligning it with the quality standards for Pb metal set by the Indonesian Ministry of Environment.	[14]
5	Coffee grounds	Carbon	Although the use of natural adsorbents chitosan and 1.4 grams of coffee grounds activated carbon can reduce arsenic, it does not meet the arsenic metal quality standards specified in Minister of Environment Regulation No. 12 of 2020. As a result, more research is needed to improve the efficiency of reducing metal arsenic.	[15]
6	Bagasse	Carbon	The optimum mass ratio of bagasse powder that can be used as an adsorbent is 0.7, with a mixing time of bagasse powder and rubber waste of 6 minutes, and the resulting adsorption	[16]

No	Waste Sources	Adsorbents type	Results	Ref
			value is 3.50235 g/g. The mass variation of filler material (2, 2.5, 3, 3.5, 4) g and the contact time (30, 60, 90, 120, 150) minutes are used in the research.	
7	Dregs tofu	Carbon	The tofu dregs waste-derived adsorbent has demonstrated its effectiveness in reducing the copper metal content in silver industrial waste. Using a magnetic stirrer, the adsorbent was brought into contact with the sample for varying durations. The atomic absorption detector analysis revealed the presence of functional groups in tofu waste, including NH (stretching), -OH, C=O, CH (aliphatic), CO, and -OH (bending vibrations). The resulting copper metal content was measured at 19.5979 ppm. The optimal adsorption period was determined to be 120 minutes, achieving an adsorption efficiency of 54.88%.	[17]
8	Rice husk	Carbon	Rice husk is an excellent adsorbent for lead metal ions, with a maximum absorption efficiency of 99%.	[18]
9	Pineapple leaf	Carbon	The adsorption equilibrium data exhibited the highest conformity with the Langmuir adsorption isotherm, with an R^2 value of 0.969 and a maximum adsorption capacity (q_{max}) of 288.34 mg/g. This study underscores the utilization of pineapple waste biomass as a cost-effective and efficient precursor material for manufacturing activated carbon, primarily aimed at eliminating colour from wastewater. Notably, the nitrogen loading rate in the ANAMMOX reactor during treatment, which stands at 2 kgN/m^3/d, is notably lower compared to that in sludge digestion wastewater, where the rate is as high as 10 kgN/m^3/d.	[19]
10	Chicken eggshell	Carbon	The best adsorption conditions used chicken eggshells with an adsorbent mass of 11 grams, a contact time of 60 minutes, and a pH of 1 with an adsorption percentage of 41.46%.	[20]
11	Clay	Silica	For the manufacture of clay-based adsorbents, it was found that the greater the HCl concentration and the longer the activation time, the greater the SiO_2/Al_2O_3 ratio, that is, at the HCl_5N concentration with a contact time of 3 hours, the SiO_2/Al_2O_3 ratio was 12.26%. Thus, the ratio increased compared to initial raw materials with a ratio of 5.59%.	[21]
12	Durian peel	Carbon	Characteristics of activated charcoal from durian peels produced based on SNI 06-3730-1995 where the water content and ash content still meet the standards while the volatile matter content and carbon content do not meet the standards.	[22]
13	Eucalyptus leaves	Silica	Eucalyptus leaf waste can be used as an adsorbent without the carbonization process.; it simply needs to be activated with an acid solution.	[23]
14	Water hyacinth	Silica	Adsorption using activated water hyacinth powder has an optimum contact time of 30 minutes at a solution concentration of 100 ml/g of 57.175 ml/g	[24]
15	Bamboo	Carbon	Activation of bamboo charcoal affects the effectiveness of Pb metal adsorption.	[25]

Nevertheless, there has been no prior investigation into the adsorption isotherm experiment for eliminating dye contaminants from aqueous solutions utilizing adsorbents sourced from Galangal Rhizomes. Curcumin solution was selected as the representative dye pollutant in this case. Galangal Rhizomes were chosen as the raw material for this study because they contain a significant amount of carbon compounds. This means that the basic structure of a Galangal Rhizomes consists of cellulose, hemicellulose, lignin,

starch, pectin, and fibre, which provide carbon. These carbon compounds make it a candidate for carbon-based adsorbents because they contain specific functional groups that attract and retain adsorbates and operational conditions that maximize these interactions [26]. Therefore, this research investigated the adsorption characteristic of Galangal Rhizomes in adsorbing curcumin solution. This research used experimental data to determine monolayer, multilayer, and cooperative adsorption behaviours. These data were subjected to calculations using ten different adsorption isotherm models, which included Freundlich, Langmuir, Hill-Deboer, Dubinin Radushkevich, Jovanovic, Temkin, Harkin-Jura, Fowler-Guggenheim, Halsey, and Flory-Huggins models. Each adsorption isotherm model was applied through a computational approach to derive model parameters that elucidate adsorption phenomena based on adsorbate concentration and the quantity of adsorbed solution per unit of adsorbent at equilibrium [26, 27]. Figure 1 shows the adsorption profiles, Figures 1(a) and 1(b) represent the multilayer and monolayer adsorption models, respectively. Figure 1 shows a potential standard isotherm adsorption model, each presenting the concept of adsorption and an example of adsorption.

The study is unique in that the adsorption characteristics of the Galangal Rhizomes-based adsorbent are determined at multiple sizes. Here, size variations (i.e., 500, 1000, and 2000 µm) were used to analyze the adsorption characteristics. By conducting this research, it is hoped that more and more people will utilize waste, especially Galangal Rhizomes waste, for something useful, especially environmental hygiene.
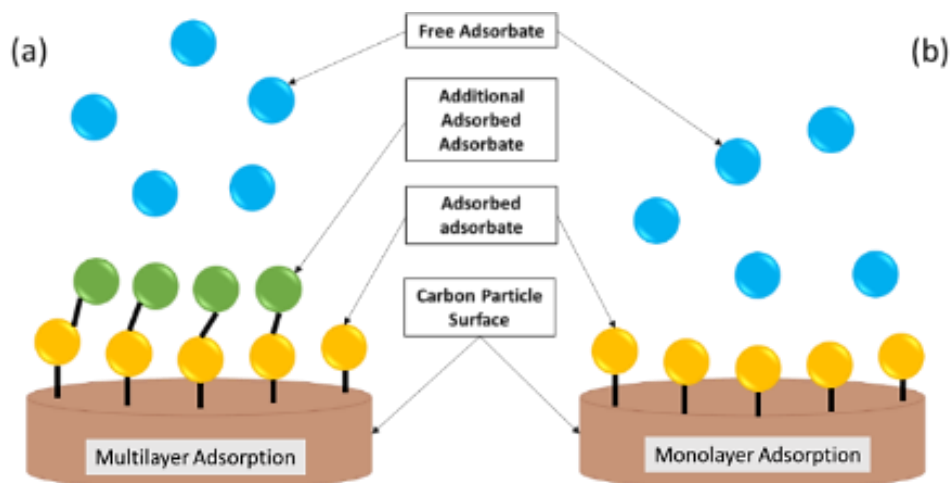

Figure 1. Illustration of the adsorption profile of (a) multilayer adsorption and (b) monolayer adsorption types

2. Adsorption Isotherm Models

2.1. Langmuir

Throughout history, various biosorbents have been evaluated and juxtaposed using the Langmuir adsorption isotherm, originally designed to elucidate the adsorption phenomenon between gas and solid

phases, primarily activated carbon [27-28]. According to the Langmuir isotherm, maximal adsorption occurs when a monolayer of adsorbate molecules is established on the adsorbent's surface. The Langmuir model posits no migratory movement of adsorbate molecules, and adsorption exclusively transpires on a stationary surface featuring uniform energy distribution [7]. The expression for the Langmuir isotherm (Eq.) can be anticipated by employing Eq. 1 and 2.

$$\frac{1}{Qe} = \frac{1}{Qmax\ KL}\ \frac{1}{Ce} + \frac{1}{Qmax} \tag{1}$$

$$RL = \frac{1}{1+KL\ Ce} \tag{2}$$

Within the Langmuir adsorption equation framework, the Langmuir adsorption constant is denoted as KL, the adsorption capacity of the monolayer as Qmax (mg/g), and the separation factor as RL. The importance of the RL parameter is elucidated in Table 2.

Table 2. The meaning of the R_L parameter

Condition	Explanation
$R_L > 1$	Adsorption is characterized by its unfavorability, which results from the occurrence of desorption.
$R_L = 1$	A linear adsorption process that does not depend on concentration.
$R_L = 0$	An irreversible adsorption process occurs when the adsorbate, common in chemisorption, cannot undergo diffusion.
$0 < R_L < 1$	Adsorption is considered favourable when there is no occurrence of desorption.

2.2. Freundlich

The Freundlich isotherm, a well-established empirical model, represents a non-ideal and reversible adsorption phenomenon that extends beyond monolayer formation, allowing for multilayer adsorption on heterogeneous surfaces characterized by varying adsorption heats and affinity distributions [28,29]. The Freundlich isotherm assumes heterogeneous adsorption sites, physical adsorption in multiple layers, and weak links. According to this hypothesis, the energy on each surface is not equal. [7]. The Freundlich isotherm model can be expressed using Eq. 3.

$$\log Qe = \log kf + \frac{1}{n}\log Ce \tag{3}$$

The equation incorporates several parameters: *n*, representing the degree of nonlinearity; *kf*, the Freundlich constant; *Ce*, the equilibrium adsorbate concentration (mg/L); and 1/*n*, signifying the adsorption strength. The specific interpretations of the parameters *n* and 1/*n* are detailed in Table 3.

Here's a breakdown of 'n' values and their interpretations: 1/*n* < 1: Normal adsorption; 1/*n* > 1: Cooperative adsorption; 1 < 1/*n* < 0: Favorable adsorption or no desorption; 0 < 1/*n* < 1: Adsorption on a

heterogeneous surface, with values closer to zero indicating increased heterogeneity of adsorbent surface.

Table 3. The meaning of the *n* and 1/*n* parameters.

Condition	Explanation
$n < 1$	Characteristics of the chemisorption adsorption process
$n = 1$	A linear adsorption process with an independent partition, uninfluenced by concentration.
$n > 1$	Attributes of the physisorption adsorption process
$1/n < 1$	The typical adsorption process
$1/n > 1$	Markers of cooperative adsorption behaviour
$1 < 1/n < 0$	Indicative of a beneficial adsorption process due to the absence of desorption
$0 < 1/n < 1$	Adsorption process occurring on varied surfaces (An approximate 1/n value close to 0 suggests heightened adsorbent surface heterogeneity).

2.3. Temkin Isotherm Model

In line with the Temkin isotherm model, all molecules have a linear decline in adsorption heat as the adsorbent surface coverage expands. A consistent dispersion of binding energies defines this particular adsorption process, reaching its peak binding energy [28, 30]. Equation 4 is the tool for calculating the adsorption heat for all molecules within the multilayer.

$$qe = \beta T\,(\ln Ce) + (BTlnAT) \tag{4}$$

The equilibrium constant for the Temkin isotherm model is denoted as A_T, and the parameter βT defines the Temkin isotherm itself. A detailed explanation of the β_T parameter can be found in Table 4.

Table 4. The meaning of the β_T parameter

Condition	Explanation
$\beta_T < 8$ kJ/mol	Physical adsorption
$\beta_T > 8$ kJ/mol	Chemical adsorption

2.4. Dubinin–Radushkevich Isotherm Model

To explain how micromaterials absorb adsorbate through a pore-filling mechanism, the Dubinin-Radushkevich isotherm model was developed. It is commonly used on heterogeneous surfaces to describe the Gaussian energy distribution adsorption mechanism [28, 31]. The adsorption potential can be used to explain the adsorption equilibrium relationship for specific adsorbate-adsorbent combinations independent of temperature. According to this model, Adsorbent size is proportional to micropore size. The Dubinin-Radushkevich adsorption equation is shown in Eq. 5.

$$lnqe = lnqs - \beta\varepsilon^2 \tag{5}$$

In the context of the Dubinin-Radushkevich isotherm, β represents the isotherm constant, ε corresponds to the Polanyi potential relative to the given conditions, and qs stands for the theoretical saturation

capacity (measured in mg/g). The Polanyi potential and the calculation of adsorption energy are provided in Equations 6 and 7, respectively.

$$\varepsilon = RT \ln \left[1 + \frac{1}{Ce} \right] \tag{6}$$

$$E = \frac{1}{\sqrt{2\beta}} \tag{7}$$

Within this context, E symbolizes the adsorption energy, indicating the free energy of sorption (expressed in kJ/mol) linked to the movement of individual sorbate molecules from the bulk solution to the solid surface. You can refer to Table 5 for precise E values.

Table 5. The meaning of the E parameter

Condition	Explanation
$E < 8$ kJ/mol	Adsorption through physical means
$E > 8$ kJ/mol	Adsorption through chemical means

2.5. Flory–Huggins Isotherm Model

The Flory-Huggins isotherm addresses the degree of adsorbate surface coverage on the adsorbent. Equation 8 provides the formula for calculating the Flory-Huggins Isotherm Model.

$$\log \frac{\theta}{C_e} = \log K_{FH} + n \log(1 - \theta) \tag{8}$$

The Flory-Huggins isotherm model [28, 32] is utilized to elucidate the viability and spontaneity of the adsorption process, signifying the reduction in the surface coverage degree from the adsorbate to the adsorbent. Here, θ denotes the extent of surface coverage, whereas KFH and nFH stand as the equilibrium constant and adsorption site, respectively. Equation 9 pertains to the equilibrium constant, KFH, which is employed to ascertain the free Gibbs energy of spontaneity.

$$\Delta G° = -RT \ln K_{FH} \tag{9}$$

A negative value for ΔG° indicates the spontaneous nature of the adsorption process, which is also influenced by temperature.

2.6. Fowler Guggenhim Isotherm Model

The Fowler-Guggenheim isotherm describes the lateral interactions among adsorbed molecules, which are contingent on the heat of adsorption that can either increase or decrease as load changes. If the interaction energy aligns positively with the force of attraction, the adsorption heat rises with loading. Conversely, there is a reduction in loading when it involves the energy repulsion of adsorbed molecules. Equation 10 provides the linear representation of this model.

$$K_{FG}C_e = \frac{\theta}{1-\theta}\exp\left(\frac{2.\theta.W}{RT}\right) \tag{10}$$

Here, W signifies the interaction energy (in kJ/mol) among the adsorbed molecules, while C_e represents the equilibrium constant, and K_{FG} corresponds to the Fowler-Guggenheim equilibrium constant. For a comprehensive understanding of the W value, please refer to Table 6.

Table 6. The meaning of the W parameter

Condition	Explanation
$W > 0$ kJ/mol	There is an exothermic attraction between the adsorbed molecules and the adsorption process.
$W < 0$ kJ/mol	An endothermic repulsion occurs between the adsorbed molecules and the adsorption process.
$W = 0$ kJ /mol	There is no interaction among the adsorbed molecules.

2.7. Hill-Deboer Isotherm Model

The Hill-de Boer isotherm characterizes dynamic adsorption and mutual interactions among adsorbed molecules, relying on model parameter values. According to this model, adsorption is a collaborative process where the capacity of one site to capture an adsorbate molecule impacts the potential of other binding sites on the same macromolecule [28, 33]. Equation 11 delineates the linear representation of this model.

$$K_1.C_e = \frac{\theta}{1-\theta}\exp\left(\frac{\theta}{1-\theta} - \frac{K_2\theta}{RT}\right) \tag{11}$$

where K_1 (L/mg) and K_2 (kJ/mol) are the energy constant of contact in the adsorbed molecular and the Hill-de Boer model, respectively. The K_2 value is described in Table 7.

Table 7. The meaning of the K_2 parameter

Condition	Explanation
$K_2 > 0$ kJ/mol	The attraction process among the adsorbed molecules is thermodynamically driven.
$K_2 < 0$ kJ/mol	The repulsion between the adsorbed molecules and the adsorption process is endothermic.
$K_2 = 0$ kJ/mol	There is no interaction among the adsorbed molecules.

2.8. Jovanovic Isotherm Model

The Jovanovic isotherm considers the potential for mechanical contact between the adsorbate and the adsorbent, incorporating the events described in the Langmuir model. The linear representation of this model is detailed in Eq. 12.

$$nQe = lnQ_{max} - K_jC_e \tag{12}$$

In this equation, Q_e represents the equilibrium adsorbate amount within the adsorbent (measured in mg/g), Q_{max} signifies the maximum adsorbate uptake, and K_J denotes the Jovanovic constant.

2.9. Harkin-jura Isotherm Model

The multilayer adsorption process described by the Harkins-Jura isotherm depends on the heterogeneous pore distribution. The linear form of this model is described in Eq. 13.

$$\frac{1}{q_e^2} = \frac{B_{HJ}}{A_{HJ}} - \left(\frac{1}{A}\right) log C_e \qquad (13)$$

The β_{HJ} value is correlated with the specific surface area of the adsorbent, while A_{HJ} represents the constants associated with the Harkin Jura isotherm.

2.10. Halsey Isotherm Model

Adsorption by multilayered adsorption processes was evaluated using the Halsey isotherm. The linear form of this model is described in Eq. 14.

$$Q_e = \frac{1}{n_H} ln K_H - \left(\frac{1}{n_H}\right) ln C_e \qquad (14)$$

where K_H dan n are the Halsey model constants.

Following adsorption theory, the process encompasses the creation of physical energy, known as physisorption, and chemical energy, termed chemisorption. Physisorption occurs when adsorbate molecules are attracted to the surface through weak forces like van der Waals interactions or other physical bonding mechanisms. These forces are generally weaker and more temporary, and the adsorbate molecules can be removed from the surface relatively easily. Physisorption typically occurs at low temperatures and low pressures. Chemisorption, conversely, entails a more robust chemical interaction between the adsorbate and the adsorbent surface. In this case, the adsorbate molecules form chemical bonds with the surface atoms, resulting in a stronger and more permanent attachment. Chemisorption typically occurs at higher temperatures and pressures [34]. Figures 2(a) and (b) depict the interactions between the adsorbent surface and the adsorbate molecules in the cases of physisorption and chemisorption, respectively. Table 8 presents the fitting curve findings along with the calculation of individual adsorption isotherm parameters.
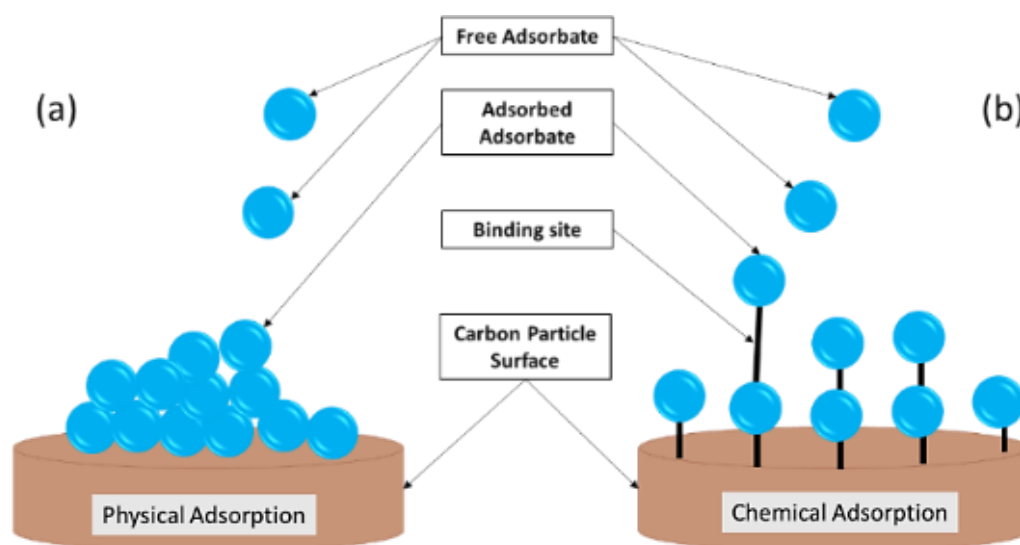

Figure 2. Illustration of the surface adsorbent-adsorbent interaction mechanism on the types of physisorption (a) and chemisorption (b)

Table 8. Adsorption isotherms fitting data, calculation, and their parameters

Isotherm Model	Linear Eq.	Plotting		Parameters
		x-Axis	y-Axis	
Langmuir	$\frac{1}{Q_e} = \frac{1}{Q_{max}K_L}\frac{1}{Ce} + \frac{1}{Q_{max}}$	$^1/_{C_e}$	$^1/_{Q_e}$	• $\frac{1}{Q_{max}} = intercept$ • $K_L = \frac{1}{Q_{max}\times slope}$
Freundlich	$\ln Q_e = \ln k_f + \frac{1}{n}\ln C_e$	lnC_e	lnQ_e	• $lnK_F = intercept$ • $\frac{1}{n} = slope$
Temkin	$q_e = B_T \ln A_T + B_T \ln Ce$	lnC_e	Q_e	• $B = slope$ • $B_T lnA_T = intercept$ • $B_T = \frac{RT}{B}$
Dubinin-Radushkevich	$\ln q_e = \ln q_s - (\beta\varepsilon^2)$	ε^2	lnQ_e	• $\beta = K_{DR} = slope$ • $E = \frac{1}{\sqrt{2\times K_{DR}}}$
Flory Huggins	$log\frac{\theta}{C_e} = logK_{FH} + nlog(1-\theta)$	$log\left(\frac{\theta}{C_0}\right)$	$log(1-\theta)$	• $n_{FH} = slope$ • $k_{FH} = intercept$ • $\Delta G^\circ = RTln(k_{FH}), \theta = 1 - \left(\frac{C_e}{C_0}\right)$
Fowler-Guggenheim	$ln\left(\frac{C_e(1-\theta)}{\theta}\right) - \frac{\theta}{1-\theta}$ $= -lnK_{FG} + \frac{2W\theta}{RT}$	θ	$ln\left[\frac{C_e(1-\theta)}{\theta}\right]$	• $W = slope$ • $-lnK_{FG} = intercept$ • $\alpha\,(slope) = \frac{2W\theta}{RT}, \theta = 1 - \left(\frac{C_e}{C_0}\right)$
Hill-Deboer	$ln\left[\frac{C_e(1-\theta)}{\theta}\right] - \frac{\theta}{1-\theta}$ $= -lnK_1 - \frac{K_2\theta}{RT}$	θ	$ln\left[\frac{C_e(1-\theta)}{\theta}\right]$ $-\frac{\theta}{1-\theta}$	• $-lnk_1 = intercept$ • $\alpha\,(slope) = \frac{k_2\theta}{RT}$ • $\theta = 1 - \left(\frac{C_e}{C_0}\right)$
Jovanovic	$lnq_e = lnq_{max} - K_J C_e$	C_e	lnQ_e	• $K_J = slope$ • $lnq_{max} = intercept$
Harkin-Jura	$\frac{1}{q_e^2} = \frac{B}{A} - \left(\frac{1}{A}\right)logC_e$	$logC_e$	$\frac{1}{q_e^2}$	• $A_H = \frac{1}{Slope}$ • $\frac{B_H}{A_H} = intercept$
Halsey	$lnQ_e = \frac{1}{n_H}lnK_H - \frac{1}{n}lnC_e$	lnC_e	lnQ_e	• $\frac{1}{n} = slope$ • $\frac{1}{n}lnK_H = intercept$

3. Materials and Method

3.1. Materials

In this study, the raw materials used to make carbon particles were Galangal Rhizomes (purchased at the local market in Cilimus, Bandung, Indonesia), amidic distilled water (purchased in Cilimus, Bandung, Indonesia), and curcumin (purchased in Cilimus, Bandung, Indonesia).

3.2. Equipment or Tools for the Adsorption Process

Some equipment is used to make a simple circuit for testing the concentration of the solution, including black cardboard (2 pcs), flashlights, vials, and the lux meter application (Android version downloaded from PlayStore). Then, the adsorption isotherm model is calculated using simple programming using Microsoft Excel software.

3.3. Carbon-based Galangal Rhizomes Preparation

The preparation of carbon particles from Galangal Rhizomes is almost the same as in previous research [7]. Galangal Rhizomes, as much as 100 grams was prepared for carbonization. Before carbonization, the Galangal was washed first, sliced thinly, and dried in the sun for 6 hours until the material dried. After that, the Galangal was carbonized in the electrical furnace at 250˚C for 9 hours. The carbonized Galangal has a particle length of 2.3 cm (23 mm). After carbonization, the carbonized Galangal Rhizomes were grounded using a saw-milled (PHILIPS 2L HR2222/30) for 5 minutes until they became powder. Furthermore, the Galangal Rhizomes powder was placed in the ASTM D1921 sieve shaker apparatus (Niaga Kusuma Lestari, Indonesia) to obtain a specific and homogeneous size. Carbon-based Galangal Rhizomes particles with particle sizes of 500, 1000, and 2000 µm were obtained using sieving (PT Rumah Publikasi Indonesia, Indonesia) with hole sizes of 55, 74, 100, 125, 200, 500, 1000, and 2000 µm (that were placed in the sieve shaker). The prepared carbon particles were then cleaned from their impurities using a centrifugation (TG16WS High-Speed Benchtop Centrifuge, Zhengzhou Hepo International Trading, Co., Ltd., China; 11,000 rpm for 5 minutes) and dried in an electrical furnace at the temperature of 80ºC to remove the physically adsorbed water.

3.4. Physicochemical Characterization

Upon preparing carbon derived from Galangal Rhizomes, a subsequent phase was involved comprehensive physical and chemical characterization. Diverse analytical methods were applied, encompassing morphological examination for particle size evaluation using a Digital Microscope (BXAW-AX-BC, China) and functional group analysis performed via Fourier Transform Infrared (FTIR) analysis using FTIR-4600 equipment from Jasco Corp, Japan, to scrutinize chemical constituents.

3.5. Batch Adsorption Process

The adsorption approach used in this study was a batch method in which 60 mL of curcumin solution was used as a model for dye solution. Curcumin solutions were prepared with different concentrations of dye molecules (100, 80, 60, 40, and 20 ppm). This study added 0.03 grams of carbon particles (as adsorbent) to 60 mL of curcumin solution (as adsorbate). The curcumin solution was then decanted for 24 hours (until the carbon settled to the batch's surface). The adsorption was conducted at room temperature, pressure, and pH (about 7). The mixture of adsorbate and adsorbent is then filtered to separate it from the adsorbent particles. Next, the adsorbate solution samples were analyzed for concentration using a lux meter (measure the maximum light intensity between the range of 3500-1000 Lux) using Lambert-Beer calculations [34]. This research was conducted on carbon-based Galangal Rhizomes sizes 500, 1000, and 2000 μm, respectively. An illustration of determining the concentration of a solution is depicted in Figure 3.
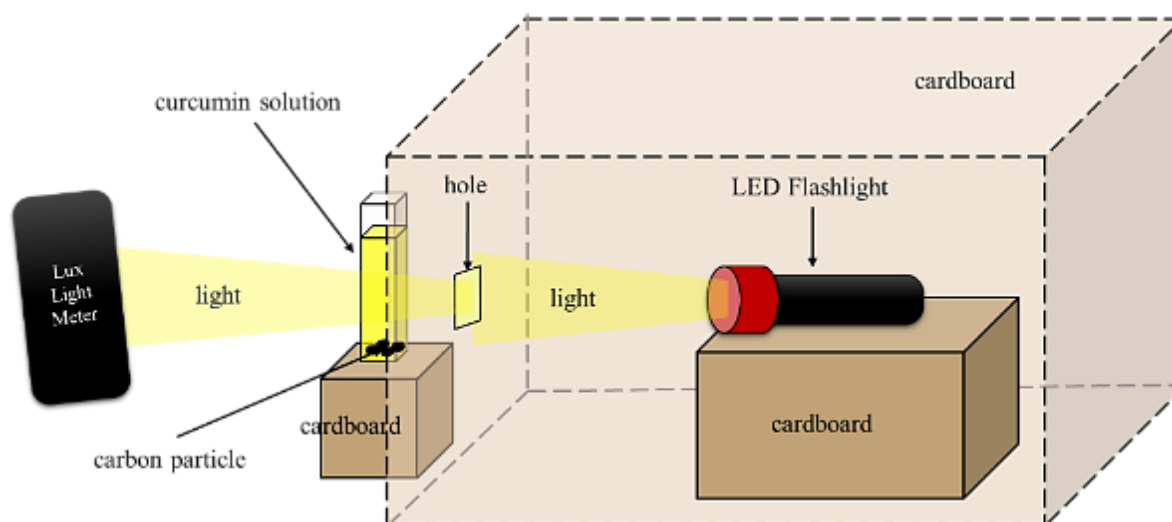
Figure 3. The carbon adsorption test involves determining the concentration of the solution after the adsorption process

4. Results and Discussion

4.1. Physicochemical Characterization of Carbon Particles

Figures 4(a) and 4(b) are images of the physical appearance of carbon using a digital microscope and ferret analysis of the particle size distribution, respectively. Figure 4(a) shows carbon particles had a heterogeneous surface. Figure 4(b) shows the carbon has sizes ranging from 89 to 2000 μm. The carbon from Galangal Rhizomes has an average size of 1058.40 μm and a standard deviation of 23.94 μm. Particle size distribution was analyzed using Ferret analysis [35].
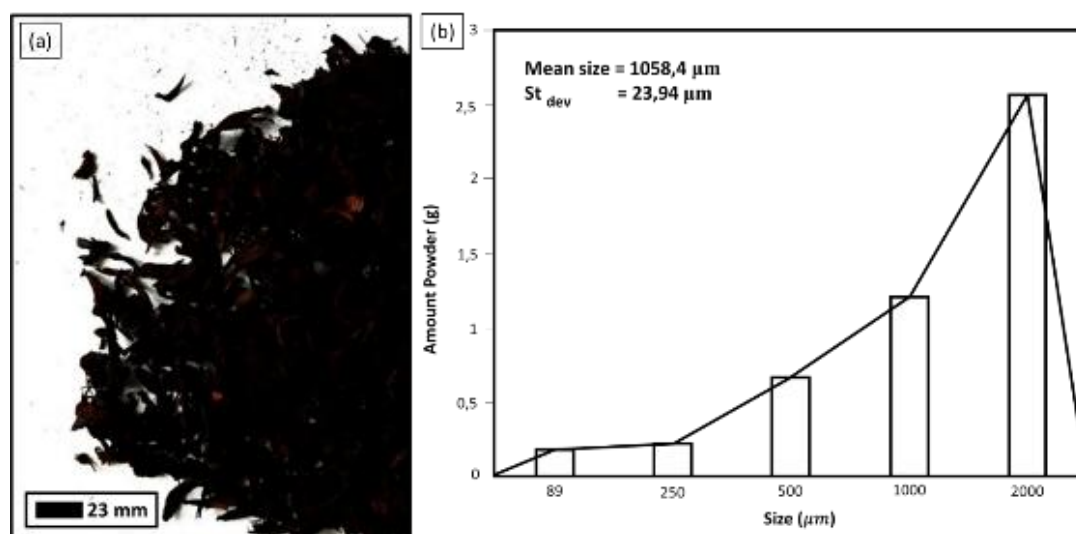
Figure 4. Digital microscopy was utilized for particle characterization of carbon (a). Ferret analysis was employed to determine particle size (b)

The findings from the FTIR analysis of carbon particles derived from Galangal Rhizomes are presented in Figure 5. Based on the data, it is possible to conclude that the structure of the carbon particles produced is identical for various particle sizes. The carbon particles exhibit a composition that comprises numerous functional groups. Among these, the hydroxyl group (OH) appears within the 3404 - 3401 cm-1 range, while functional groups associated with carbonyl compounds (including ketones and carboxylic acids) are observed between 1707 - 1718 cm^{-1}. Notably, the spectrum displays three peaks spanning the 1000 to 1750 cm^{-1} range, indicating the presence of Si-O-C. Additionally, absorption bands emerge at 468, 1103, and 1419 cm^{-1}, corresponding to saturated and unsaturated compounds.

Figure 5. FTIR analysis of carbon particles of various sizes extracted from Galangal Rhizomes

The prepared particles were in carbon materials, according to FTIR analysis. Based on the FTIR results, the treatment of particle size variations does not affect the FTIR results. Material crystallinity does not play a role in the adsorption process; instead, the adsorption processes depend entirely on the structural characteristics of carbon particles.
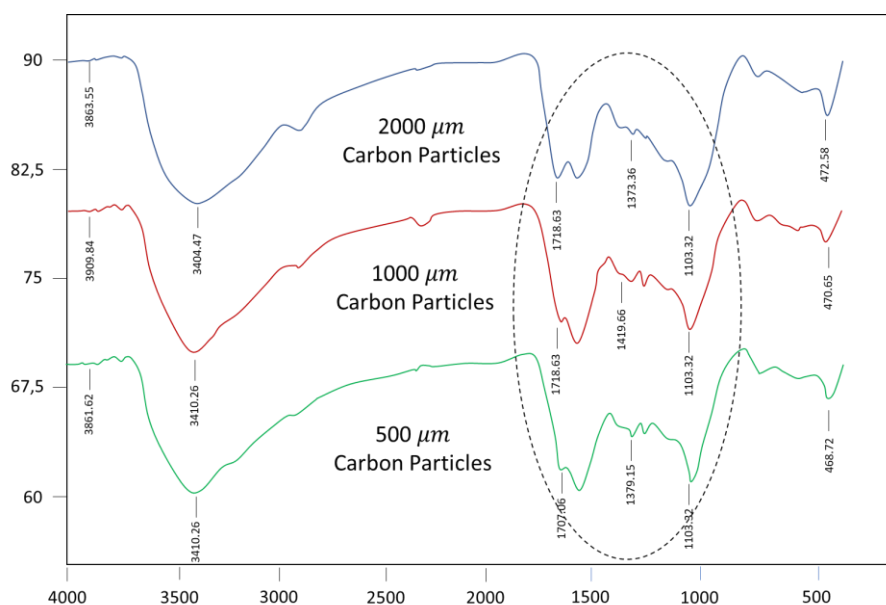
The current study focuses on establishing a basic understanding of the material through digital microscopy and Fourier transform infrared spectroscopy. This approach was chosen because both techniques provide important and direct information related to the physical and chemical properties of materials that are key in adsorption. The focus on the theoretical aspects allows the establishment of a strong theoretical foundation for an in-depth understanding of surface dynamics and molecular interactions that identifies new strategies to improve adsorption efficiency, such as modifying the adsorbent surface or regulating process conditions. Indeed, it is important to integrate additional materials characterization techniques such as surface area analysis, elemental analysis, and pore size distribution measurements to gain a more comprehensive understanding of the physicochemical properties of the materials studied so that characterization will be performed in the future.

4.2. Characteristics of Adsorption of Carbon Particles Based on Isotherm Models

Employing the adsorption isotherm methodology analyses the adsorption mechanism and reveals the adsorbent's attributes and traits. The adsorption isotherm fit comparison data were compared based on the correlation coefficient (R^2) and other relevant parameters of each isotherm model against the experimental data. The correlation coefficient (R^2) value plays a pivotal role in assessing adsorption characteristics, with a higher R^2 value signifying a closer alignment of the adsorption isotherm model with the actual adsorption behavior. In summary, analyzing the fit of the adsorption process through R^2 values of adsorption isotherm models is a common approach to understanding how adsorbates interact with adsorbents. By comparing the R^2 values of various isotherm models, we can determine which model best describes the observed adsorption system. R^2 values close to 1 indicate that the model represents the experimental data well. To explore this further, the adsorption data was graphed against four linear adsorption isotherm models, including Freundlich, Langmuir, Dubinin-Radushkevich, and Temkin. The Fowler Guggenheim, Flory Huggins, Jovanovic, Hill Deboer, Halsey, and Harkin Jura models were employed to fit the adsorption data, examining their compatibility with adsorption properties. A significant match between adsorption properties and the models was established when the R^2 value surpassed the threshold of 0.70. Table 9

comprehensively presents the outcomes derived from the adsorption analysis, including the correlation coefficient value (R^2) and various isotherm parameters. These findings were meticulously juxtaposed against ten different adsorption isotherm models.

A series of repeated experiments for each sample was conducted to ensure the accuracy and reliability of the adsorption isotherm analysis results. This approach enabled the identification and minimisation of data variability that may arise from fluctuations in experimental conditions or measurement errors. After performing this analysis several times per sample, the data set that showed the best consistency was used in the isotherm data matching process. A simple data linearisation process described in Table 8 was performed to facilitate linear regression analysis and improve understanding of adsorbate-adsorbent interactions. This linearisation was performed based on mathematical transformations appropriate for each isotherm model tested, such as Langmuir, Freundlich, and Temkin. This process made it possible to apply the linear regression method, widely recognized for its practicality in evaluating the fit of isotherm models to experimental data.

Table 9 displays the correlation coefficient values for each adsorption isotherm model. The following is a detailed explanation of the results of the adsorption isotherm model. The Langmuir isotherm model was obtained from the results of plotting $1/C_e$ and $1/Q_e$ (see Table 8) using Eq. 1. The Langmuir model adequately represents the suitability of the adsorption equilibrium experimental data on adsorption systems with adsorbents that have relatively large particle sizes (1000 and 2000 µm) because $R^2 > 0.70$, which confirms that the adsorption occurs via monolayer formation. The formation of a monolayer indicates that the adsorption process occurs on a homogeneous surface [36]. The Langmuir adsorption model did not show suitability for an adsorption system with an adsorbent having a particle size of 500 µm because the R^2 value < 0.70, indicating that the adsorption did not follow the formation of a monolayer. In the adsorbent system using a particle size of 500 µm, the adsorption process is multilayer, in which the multilayer appears to be primarily controlled by the degree of surface roughness characteristic of the microporous adsorbent. Langmuir parameter values for all adsorption systems (that is, Q_{max}, R_L, and K_L) are listed in Table 9. Maximum adsorption capacity (Q_{max}) and binding energy constant (K_L) values were estimated from the Langmuir model for adsorption systems with adsorbent sizes of 500, 1000, and 2000 µm are 0.2632, 0.2315 and 0.1908 mg/g, and 11.058, 10.482 and 8.853 L/mg, respectively. K_L quantifies the adsorbate's attraction to the adsorbent, with a high K_L value signifying a strong affinity between the adsorbate and the adsorbent

surface [36]. The R_L value within the Langmuir model confirms that the adsorption process is advantageous (typical adsorption) for all the adsorption systems.

Equation 3 was employed within the framework of the Freundlich model, which was established by plotting lnC_e against lnQ_e adsorption data, as detailed in Table 8. The parameter values for the Freundlich model (K_F, n_F, and $1/n$) are presented in Table 9.

The Freundlich model is designed to elucidate how adsorption results in layered formations, attributed to the heterogeneity of adsorbent surfaces possessing diverse energy distributions. It is important to note that the Freundlich isotherm model does not align with the experimental adsorption data for the 500 µm adsorbent system, as indicated by the lower R^2 value ($R^2 < 0.70$). However, this model effectively explains adsorption systems' appropriateness for 1000 and 2000 µm adsorbents.

Based on these findings, it can be inferred that the Freundlich model assumes that the adsorption process at relatively large adsorbent particle sizes (1000 and 2000 µm) follows a multilayer formation, whereas it does not exhibit a multilayer formation for adsorption processes involving relatively smaller particle size adsorbents (500 µm). Furthermore, the experimental observation of $1/n < 1$ confirms the favourable nature of the adsorption process. The K_F parameter indicates adsorption capacity, whereas a low value indicates low adsorption capacity and vice versa [37]. The n_F value obtained in this study was more than one, indicating the role of physical processes in adsorption.

The linear fitting of the Temkin isotherm model was obtained from the lnC_e vs Q_e plot (see Table 8) according to Eq. 4, which describes the Temkin isotherm, which postulates that the heat of adsorption diminishes linearly throughout the adsorption process, leading to a consistent dispersion of binding energy [38]. It is worth noting that the Temkin isotherm model is not well-suited for depicting experiments in adsorption systems characterized by relatively small particle sizes (500 µm) due to an R^2 value of less than 0.70. However, Temkin's model is compatible with adsorption systems using relatively large adsorbents (1000 and 2000 µm). Due to fitting this model, it was confirmed that the adsorption system using relatively large adsorbent particle sizes (1000 and 2000 µm) exhibits energetic heterogeneity of the adsorption sites. That is, adsorption occurs at heterogeneous sites. Parameter values indicating maximum bond energy indicate physical adsorption ($\beta_T < 8$ kJ/mol, physisorption) [39].

The Dubinin-Radushkevich model was derived from fitting the adsorption data using Eq. 5. This isotherm expresses the adsorption mechanism onto a heterogeneous surface. Experimental data with 1000

and 2000 µm adsorbents showed a very good fit with this isotherm model based on the R^2 value compared to the adsorption system using relatively small particle sizes (500 µm). Consequently, the adsorption to surface energy heterogeneity with the 1000 and 2000 µm adsorbents followed the pore volume filling mechanism. Analysis of the E values revealed that $E < 8$ kJ/mol, confirming that this type of adsorption occurred via a physical process [38].

The Flory-Huggins isotherm model anticipates a stratified adsorption process contingent upon the adsorbent pore surface, as represented by Equation 8. When examining the value of R^2 in the context of the Flory-Huggins model, it is observed that for particle sizes of 500 and 2000 µm, the value remains below 0.70. This suggests that the adsorption process primarily occurs in a multilayer fashion.

In contrast, at a particle size of 1000 µm, the R^2 value surpasses 0.70, signifying that the adsorption process unfolds in a multilayer manner. In this scenario, the adsorbate occupies more than one adsorbent zone, and the adsorption process transpires spontaneously, as corroborated by the negative value of the n_{FH} parameter.

The Fowler-Guggenhim model, represented by Eq. 10. The Fowler-Guggenheim isotherm, dependent on the heat of adsorption and can change positively or negatively with loading, is used to determine the lateral contact of the adsorbed molecule. The Fowler-Guggenhim model is known to be inversely proportional to the Harkin-Jura model when viewed from the R^2 value. In the Fowler-Guggenhim model, it is known that the value of R^2 at a particle size of 500 and 1000 µm is more than 0.70, indicating that adsorption occurs in a monolayer manner. Meanwhile, adsorption occurs in a multilayer condition at a particle size of 2000 µm at the value of $R2 < 0.70$. The interactions shown in the Fowler-Guggenhim model between the adsorbed molecules are repulsive, indicating that the interactions are endothermic, which is confirmed by the negative value of W.

The Hill-Deboer model, represented by Eq. 11, is only compatible with adsorption systems studied using large particle sizes (1000 and 2000 µm), indicating that adsorption interactions are bilateral (multilayer) [40]. The adsorption mechanism occurs in a monolayer in two adsorption systems that use carbon with a relatively small (500 µm). The adsorbate-adsorbent interaction, represented by the value of K_2 in all adsorption systems, namely $K_2 < 0$, indicates a repulsive interaction between the adsorbed molecules.

The Jovanovic model was derived from fitting the C_e vs lnQ_e data (see Table 8) using Eq. 12. The

Jovanovic model is similar to the Langmuir isotherm model, which includes interactions on a homogeneous surface. The Jovanovic isotherm, which describes the adsorption of lateral interactions, was found to be most suitable for adsorption systems using 1000 and 2000 µm adsorbents. For the other adsorption systems (500 µm), on the other hand, it represents heterogeneous adsorption.

The Harkin-Jura model is obtained using Eq. 13. In Table 3, based on the Harkin-Jura model, it can be seen that the R^2 value at 500 µm is 0.04826, at 1000 µm is 0.93849, and at 2000 µm is 0.85916. Based on the R^2 value, it is known that the adsorption process on 500 µm particles occurs in a monolayer. Meanwhile, particle sizes of 1000 and 2000 µm occur through the formation of multilayers.

The Halsey model is obtained from the lnC_e vs lnQ_e plot of Eq. Figure 14 shows the suitability of adsorption systems using relatively large adsorbent particle sizes (1000 and 2000 µm) because the R^2 value is more than 0.90. However, this model is unsuitable for adsorption systems using relatively small adsorbent particle sizes (500 µm). Utilizing the Halsey isotherm model, one can assess a multilayer adsorption system, particularly for the adsorption of curcumin occurring at a considerable distance from the surface [41]. The efficacy of the Halsey isotherm model in matching the experimental data stems from the heterogeneous distribution of activation sites and the multilayer adsorption process of carbon in systems employing relatively larger particle sizes [37].

Table 9. Models of isotherm adsorption in this study

Model	Parameter	Particle size (µm)			Notes
		500	**1000**	**2000**	
Langmuir	R_L	0.0083	0.0260	0.0312	The adsorption is favorable
	Q_{max} ($\frac{mg}{g}$)	0.2632	0.2315	0.15312	The maximum adsorption capacity of the adsorbent
	K_L (L/mg)	11.058	10.399	1.7601	The weak interaction between adsorbate and adsorbent is shown by the small value of the Langmuir constant.
	R^2	0.0274	0.96277	0.93886	$R^2 > 0.7$ *is monolayer* $R^2 < 0.7$ *is multilayer*
Freundlich	K_F	1.6918	1.51481	1.0569	The adsorption capacity of the adsorbent
	$\frac{1}{n_F}$	0.055	0.41529	0.5076	Close to 0, indicating favorable adsorption
	n_F	2.3025	2.40796	0.9911	above 1, shown Physisorption
	R^2	0.0444	0.97126	0.93645	$R^2 > 0.7$ *is multilayer* $R^2 < 0.7$ *is monolayer*
Temkin	β_T (J/mol)	2.2228	0.32200	0.15891	Physisorption ($\beta_T < 8$ kJ/mol)

Model	Parameter	Particle size (μm)			Notes
		500	**1000**	**2000**	
	A_T (L/g)	88.0487	78.30132	-2132.871	Temkin equilibrium binding constant
	R^2	0.04543	0.96472	0.92432	Homogenous adsorbate in the adsorbent surface ($R^2 < 0.90$)
Dubinin-Radush-kevich	β (K_{DR})	0.0002	0.1165	0.0175	The constant of the Dubinin-Radushkevich isotherm
	E	0.0496739	0.0422355	0.04082482	Physisorption ($E < 8$ kJ/mol)
	R^2	0.06148	0.83162	0.94684	$R^2 > 0.7$ is multilayer $R^2 < 0.7$ is monolayer
Flory-Hug-gins	n_{FH}	-0.2330	-1.0187	-0.5932	Under 1, the adsorbate takes more than one adsorbent zone
	K_{FH}	0.0071	0.00071	0.0111	The constant of the Flory-Huggins isotherm
	$\Delta G°$	-121.429	-176.771	-300.3857	Under 0, the adsorption process is spontaneous
	R^2	0.0049	0.95257	0.02712	$R^2 > 0.7$ is monolayer $R^2 < 0.7$ is multilayer
Fowler-Guggen-heim	K_{FG}	1.4×10^{-58}	8.7×10^{-11}	0.00063081	The constant of the Fowler-Guggenheim isotherm
	W	-1.0205	-32.209	-4.7118	Under 0, interactions between the adsorbed molecules repulsive are endothermic
	R^2	0.93749	0.96358	0.05131	$R^2 > 0.7$ is multilayer $R^2 < 0.7$ is monolayer
Hill-Deboer	k_2	-1.145	-4.174	-0.6885	Under 0, interactions between the adsorbed molecules repulsive is endothermic
	R^2	0.62279	0.91379	0.80524	$R^2 > 0.7$ is multilayer $R^2 < 0.7$ is monolayer
Jovanovic	K_J	0.0521	0.0397	0.0392	The constant of the Jovanovic isotherm
	Q_{max}	165.5231	121.7594	54.9724	Maximum absorption of adsorbate
	R^2	0.28091	0.86641	0.91799	$R^2 > 0.7$ is multilayer $R^2 < 0.7$ is monolayer
Harkin-Jura	A_H	-1.2574	-1.5858	-1.2098	The constant of the Harkin-Jura isotherm.
	B_H	0.0000345	0.0000929	0.00015	Correlated to the surface area of the adsorbent
	R^2	0.04826	0.93849	0.85916	$R^2 > 0.7$ is multilayer $R^2 < 0.7$ is monolayer
Halsey	n_H	2.5678	2.4079	0.9911	The isotherm constant of Halsey
	K_H	8.8002	5.1487	5.905	The constant of the Halsey isotherm
	R^2	0.0444	0.97126	0.93645	$R^2 > 0.7$ is multilayer $R^2 < 0.7$ is monolayer

Based on the previous explanation, in detail, the suitability of each isotherm adsorption model is summarised in Table 10. The model suitable for each size variation of the adsorbent is marked with a "match" word.

Table 10. Detailed suitability of each adsorption isotherm model

Model	Particle Size			Note
	2000	1000	500	
Langmuir	match	Match	-	• Large-size carbon (2000 and 1000 µm) follows monolayer formation • Small-size carbon (500 µm) follows multilayer formation
Freundlich	Match	Match	-	• Large-size carbon (2000 and 1000 µm) follows multilayer formation • Small-size carbon (500 µm) follows monolayer formation
Temkin	Match	Match	-	• Large-size carbon (2000 and 1000 µm) follows monolayer formation • Small-size carbon (500 µm) follows multilayer formation
Dubinin-Radush-kevich	Match	Match	-	The pore-filling mechanism in the adsorbent surface (multilayer formation) for large-size adsorbent
Flory-Huggins	-	Match	-	• Only adsorbent with 1000 µm follows multilayer formation • Particles of 2000 and 500 µm follow the monolayer formation
Fowler-Guggen-heim	-	Match	match	• Medium and small-size carbon (1000 and 500 µm) follows monolayer formation • Large-size carbon (2000 µm) follows multilayer formation
Hill-Deboer	-	Match	match	• Large-size carbon (2000 and 1000 µm) follows multilayer formation • Small-size carbon (500 µm) follows monolayer formation
Jovanovic	Match	Match	-	• Large-size carbon (2000 and 1000 µm) follows monolayer formation • Small-size carbon (500 µm) follows multilayer formation
Harkin Jura	Match	Match	-	• Large-size carbon (2000 and 1000 µm) follows multilayer formation • Small-size carbon (500 µm) follows monolayer formation
Halsey	Match	Match	-	• Large-size carbon (2000 and 1000 µm) follows multilayer formation • Small-size carbon (500 µm) follows monolayer formation

Finally, we can summarise the adsorption mechanism of curcumin on Galangal Rhizomes-based carbon adsorbents for small-sized adsorbents following the formation of monolayers. Meanwhile, the adsorbents with medium and large sizes follow the formation of multilayers. Furthermore, the adsorption mechanisms for large particle size adsorbent studied systems are favourable adsorption and pore filling and attractive interactions between adsorbates through physical force (physisorption). The adsorption mechanism for adsorption systems using adsorbents with relatively small particle sizes also follows favorable adsorption and attractive interactions between adsorbates through physical force. However, the adsorption mechanism does not follow pore filling. Monolayer formation occurs without interacting with adsorbed molecules and involves uniform energy distribution on the surface, resulting in no adsorbate transmigration [38].

Conversely, multilayer adsorption occurs due to the heterogeneous energy distribution at the active sites of the adsorbent [42]. All weak electrostatic interactions, including van der Waals forces, dipole-dipole interactions, and London dispersion forces, fall under the category of physisorption. The energy needed to establish these weak physisorption interactions between the adsorbate and substrate typically ranges from 0.2 to 4.0 kJ/mol, representing the lowest and most easily disrupted interactions. Adsorption that occurs beyond monolayer and multilayer formation results from the binding energy associated with physisorption characteristics, primarily driven by Van der Waals forces. The primary contributors to monolayer formation are geometric irregularities and energy disparities within the surface profile. A detailed proposed adsorption mechanism based on the adsorption isotherm model is illustrated in Figures 6(a) and (b).
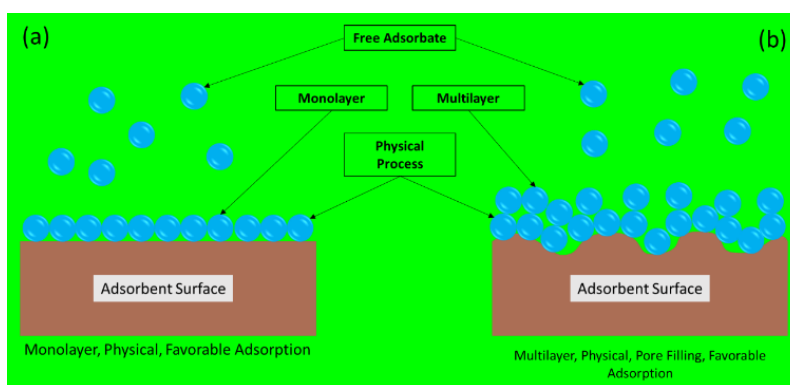

Figure 6. Illustration of adsorption process for small particle (a) and large particle (b)

The results of this study also revealed that particle size influences adsorption ability. In theory, smaller particles should have greater adsorption effectiveness than larger ones [43]. This is because smaller particle size directly promotes greater surface area, which results in better adsorption ability [38]. However, experimental results show that carbon particles with a diameter of 500 m are less efficient at adsorption than larger carbon particles (1000 and 2000 μm). Small particle collisions and aggregation pose significant challenges. Such aggregation tendencies result in larger particles [44], which have a lower surface area and adsorption capacity and thus act as impurities in the adsorption system (as evidenced by the incompatibility of most isotherm models). The reduced size of the carbon makes the subsequent separation process more difficult, resulting in impurities.

Each of these adsorption isotherms has advantages and disadvantages, primarily because each isotherm is tailored to describe specific adsorption phenomena, allowing for accurate adsorption characteristics. For instance, the Langmuir and Freundlich isotherms, two widely used two-parameter models, exemplify this concept. The Langmuir isotherm is suitable for describing monolayer adsorption

occurring on homogeneous sites, while the Freundlich isotherm applies to multilayer adsorption on heterogeneous sites. Therefore, analyzing other parameters, such as energy interactions between adsorbates and pores, requires using other isotherm models. Therefore, in this study, we modelled ten adsorption isotherms.

Indeed, this study asserts that the effectiveness of this material in adsorbing dyes from aqueous solutions should be evaluated as a first step in exploring its possible applications in wastewater treatment. Based on this study, carbon particles from galangal rhizomes show significant potential for applications in colour effluent removal, mainly due to their properties, such as large surface area and availability of functional groups that can interact with dye molecules [26]. This is promising for applications in the textile industry, where colour effluents constitute a significant problem, and in other sectors that use dyes and pigments. This research may have limitations in some scenarios, including:

(i) Stability: In its natural form, Galangal Rhizomes have a higher tendency to decompose, which may limit their application and effectiveness as an adsorbent. However, the natural transformation to the activated carbon form marks a substantial increase in the material's stability, making it more resistant to decomposition and increasing its adsorptive application potential under various environmental conditions. This change in stability is attributed to the carbonization and activation processes that alter the structure and chemical composition of Galangal Rhizomes. This process results in a material with high porosity, large surface area, and, most importantly, significant resistance to decomposition and other external factors. In addition, studies examining the stability of adsorbents under various operational and environmental conditions, including pH, time, temperature, adsorbate concentration, and adsorbent dosage, are important steps in validating their effectiveness and applicability in real-world scenarios.

(ii) Regeneration: This regeneration potential and the previously discussed stability place Galangal Rhizomes-based carbon adsorbent as a promising candidate for practical and sustainable waste treatment applications.

(iii) Adsorbent Performance under Real Conditions: This study also simplified the complexity of real-world applications as the adsorption process was carried out by adopting turmeric as a model adsorbate since it is based on the suitability of its molecular size (1.4 nm) with various types of dye molecules commonly used in industry. Real effluent mixtures can contain various dye molecules with different characteristics [45]. However, the choice in this experiment made it possible to specifically explore and understand the adsorption mechanisms present, providing a solid foundation for broader adsorption

theory and practice.

Based on some of the limitations that have been revealed, it becomes a direction for further research that can be carried out.

5. Conclusion

This study aimed to conduct adsorption isotherm experiments using carbon microparticles derived from Galangal rhizomes. Utilizing Galangal rhizomes as a source of carbon not only provides a sustainable adsorbent material and offers environmental benefits. The carbon particles derived from these rhizomes effectively remove dyes from curcumin solutions, resulting in clearer and purer outcomes. We employed the batch reactor technique to investigate the adsorption isotherm model, with curcumin as the model dye. The findings suggest that adsorption occurs differently based on the size of the carbon substrate: larger substrates facilitate multilayer formation, while smaller ones lead to monolayer formation. The multilayer creation is due to the heterogeneous surface of the adsorbent, stemming from the pore-filling process, whereas the monolayer formation is based on the adsorbent's surface structure.

All adsorption systems operate through normal adsorption with physical interactions. Given its carbon content, Galangal rhizome-based carbon demonstrates significant potential as an adsorbent. While this study focused on removing dyes from curcumin solutions, future research could explore its efficacy in removing other dye types, broadening its applications. Optimizing contact time, adsorbent dosage, pH, and temperature could enhance adsorption efficiency. Characterizing the adsorbent's surface area, pore size distribution, and chemical composition would provide insights into the adsorption mechanism. Overall, the versatility of the adsorption process makes Galangal rhizome-derived carbon a promising candidate for wastewater treatment, with further exploration needed for other potential raw materials and their characteristics.

Declaration of Competing Interest: The authors declare they have no known competing interests.

References

[1]   I. E. Wijayanti, E. A. Kurniawati, S. Solfarina, "Studi kinetika adsorpsi isoterm persamaan langmuir dan freundlich pada abu gosok sebagai adsorben. *EduChemia (Jurnal Kimia dan Pendidikan)*, vol. 4(2), pp. 175-184, 2019.

[2]   F. Hanum, R. J. Gultom, M. Simanjuntak, "Adsorpsi zat warna metilen biru dengan karbon aktif dari kulit durian menggunakan KOH dan NAOH sebagai aktivator," *Jurnal Teknik Kimia USU*, vol. 6(1), pp. 49-55, 2017.

[3]   A.M. Anshar, P. Taba, I. Raya, "Kinetic and thermodynamics studies the adsorption of phenol on activated carbon from

rice husk activated by ZnCl2," *Indonesian Journal of Science and Technology*, vol. 1(1), pp. 47-60, 2016.

[4]   R.H. Khuluk, A. Rahmat, "Removal of methylene blue by adsorption onto activated carbon from coconut shell (Cocous nucifera L)," *Indonesian Journal of Science and Technology*, vol. 4(2), pp. 229-240, 2019.

[5]   S.R. Putri, S.N. Hofifah, G.C.S. Girsang, A.B.D. Nandiyanto, "How to identify misconception using certainty of response index (CRI): A study case of mathematical chemistry subject by experimental demonstration of adsorption," *Indonesian Journal of Multidiciplinary Research*, vol. 2(1), pp. 143-158, 2022.

[6]   A.B.D. Nandiyanto, Z.A. Putra, R. Andika, M. R. Bilad, T. Kurniawan, R. Zulhijah, I. Hamidah, "Porous activated carbon particles from rice straw waste and their adsorption properties," *Journal of Engineering, Science and Technology*, vol. 12(Special Issue 10), pp. 1-11, 2017.

[7]   A.B.D. Nandiyanto, R. Maryanti, M. Fiandini, R. Ragadhita, D. Usdiyana, S. Anggraeni, W.R. Arwa, A. S. M. Al-Obaidi, "Synthesis of carbon microparticles from red dragon fruit (Hylocereus undatus) peel waste and their adsorption isotherm characteristics," *Molekul*, vol. 15(3), pp. 199-209, 2020.

[8]   M. Fiandini, R. Ragadhita, A. B. D. Nandiyanto, W. C. Nugraha, "Adsorption characteristics of submicron porous carbon particles prepared from rice husk," *Journal of Engineering Science and Technology*, vol. 15, pp. 022-031, 2020.

[9]   I. Rahmawati, R. Intan, M. Zakaria, "Photoluminescence study of carbon dots from ginger and galangal herbs using microwave technique," *In Journal of Physics: Conference Series*, vol. 985(1), pp. 012004, 2018.

[10]   M. Hema, S. Arivoli, "Comparative study on the adsorption kinetics and thermodynamics of dyes onto acid activated low cost carbon," *International Journal of Physical Sciences*, vol. 2(1), pp. 10-17, 2007.

[11]   A. Rahma, "Pengaruh pra-perlakuan adsorpsi karbon aktif terhadap fouling membran Ultrafiltrasi Polisulfon (Uf-Psf) Pada penyisihan Bahan Organik Alami (BOA) air gambut," *Jernih: Jurnal Tugas Akhir Mahasiswa*, vol. 1(2), pp. 1-16, 2018.

[12]   S. Singh, A. Kumar, H. Gupta, "Activated banana peel carbon: A potential adsorbent for Rhodamine B decontamination from aqueous system," *Applied Water Science*, vol. 10(8), pp. 1-8, 2020.

[13]   M. N. Dewi, H. R. Triuswatun, "Pemanfaatan Limbah Daun Jati (Tectona Grandis LF) Sebagai Adsorben Alami Dalam Penurunan Kadar Free Fatty Acid Minyak Jelantah," *Applicable Innovation of Engineering and Science Research (AVoER)*, pp. 298-301, 2019.

[14]   D. Suwazan, N. Nurhidayanti, "Efektivitas Kombinasi Kitosan dan Ampas Teh Sebagai Adsorben Alami dalam Menurunkan Konsentrasi Timbal Pada Limbah Cair PT PXI," *Jurnal Ilmu Lingkungan*, vol. 20(1), pp. 37-44, 2022.

[15]   N. Nurhidayanti, N. I. Ilyas, and D. Suwazan, "Efektivitas Kombinasi Kitosan dan Ampas Kopi sebagai Adsorben Alami dalam Menurunkan Konsentrasi Arsen Pada Limbah Cair PT PXI," *Jurnal Tekno Insentif*, vol. 15(2), pp. 76-87, 2021.

[16]   F. Ali, A. R. Fithri, R. H. Adhitya, "Pemanfaatan limbah karet alam dan ampas tebu sebagai adsorben crude oil spills," *Jurnal Teknik Kimia*, vol. 23(1), pp. 9-16, 2017.

[17]   D. R. Indah, H. Hatimah, H. Hulyadi, "Efektivitas ampas tahu sebagai adsorben logam tembaga pada air limbah industri," *Hydrogen: Jurnal Kependidikan Kimia*, vol. 9(2), pp. 57-66, 2021.

[18]   W. Wardalia, "Karakterisasi pembuatan adsorben dari sekam padi sebagai pengadsorp logam timbal pada limbah cair," *Jurnal Integrasi Proses*, vol. 6(2), pp. 184-185, 2016.

[19]   M. N. Mahamad, M. A. A. Zaini, Z. A. Zakaria, "Preparation and characterization of activated carbon from pineapple waste biomass for dye removal," *International Biodeterioration and Biodegradation*, vol. 102, pp. 274-280, 2015.

[20]   T. Nurlaili, L. Kurniasari, R. D. Ratnani, "Pemanfaatan limbah cangkang telur ayam sebagai adsorben zat warna methyl orange dalam larutan," *Jurnal Inovasi Teknik Kimia*, vol. 2(2), pp. 11-14, 2017.

[21]   L. U. Widodo, S. Najah, C. Istiqomah, "Pembuatan adsorben berbahan baku tanah liat dari limbah industri pencucian pasir silika dengan perbedaan konsentrasi hcl dan waktu aktivasi," *Journal of Research and Technology*, vol. 6(1), pp. 10-15, 2020.

[22] B. Yusuf, "Pemanfaatan arang aktif dari kulit durian (Durio Zibethinus L.) sebagai adsorben ion logam kadmium (II)," *Jurnal Kimia Mulawarman*, vol. 13(1), pp. 23-27, 2016.

[23] D. I. P. Kusumaningrum, D. H. A. Sudarni, S. Wahyuningsih, "Optimasi pengaruh waktu kontak dan dosis adsorben limbah daun kayu putih (melaleuca cajuputi) dengan metode isoterm adsorpsi langmuir," *Jurnal Teknik Kimia USU*, vol. 11(2), pp. 72-79, 2022.

[24] M. A. Rochman, C. Saleh, B. Yusuf, "Pemanfaatan serbuk eceng gondok (Eichornia crassipes) teraktivasi dengan sistem kantong celup sebagai adsorben penjerap ion logam kadmium (Cd)," *Jurnal Atomik*, vol. 2(2), pp. 197-203, 2017.

[25] T. Widayatno, "Adsorpsi logam berat (Pb) dari limbah cair dengan adsorben arang bambu aktif," *Jurnal teknologi bahan alam*, vol. 1(1), pp. 17-23, 2017.

[26] V. Chairgulprasert, A. Japakeya, H. Samaae, "Phytoremediation of synthetic wastewater by adsorption of lead and zinc onto Alpinia galanga Willd," *Songklanakarin Journal of Science & Technology*, vol. *35*(2), pp. 227-233, 2013.

[27] J. Romero-Gonzalez, J. R. Peralta-Videa, E. Rodrıguez, S. L. Ramirez, J. L. Gardea-Torresdey, "Determination of thermodynamic parameters of Cr (VI) adsorption from aqueous solution onto Agave lechuguilla biomass," *The Journal of chemical thermodynamics*, vol. 37(4), pp. 343-347, 2005.

[28] R. Ragadhita, A.B.D. Nandiyanto, "How to calculate adsorption isotherms of particles using two-parameter monolayer adsorption models and equations," *Indonesian Journal of Science and Technology*, vol. 6(1), pp. 205-234, 2021.

[29] H. Freundlich, "Über die adsorption in lösungen," *Zeitschrift für physikalische Chemie*, vol. 57(1), pp. 385-470, 1907.

[30] M. I. Temkin, "Kinetics of ammonia synthesis on promoted iron catalysts," *Acta physiochim*. URSS, vol. 12, pp. 327-356, 1940.

[31] A. Dąbrowski, "Adsorption—from theory to practice," *Advances in Colloid and Interface Science*, vol. 93(1-3), pp. 135-224, 2001.

[32] M. H. Jnr, A. I. Spiff, "Equilibrium sorption study of Al3+, Co2+ and Ag+ in aqueous solutions by fluted pumpkin (Telfairia occidentalis HOOK f) waste biomass," *Acta Chim. Slov*, vol. 52, pp. 174-181, 2005.

[33] D. Ringot, B. Lerzy, K. Chaplain, J. P. Bonhoure, E. Auclair, Y. Larondelle, "In vitro biosorption of ochratoxin A on the yeast industry by-products: Comparison of isotherm models," *Bioresource Technology*, vol. 98(9), pp. 1812-1821, 2007.

[34] R.A. Pratiwi, A.B.D. Nandiyanto, "How to read and interpret UV-VIS spectrophotometric results in determining the structure of chemical compounds," *Indonesian Journal of Educational Research and Technology*, vol. 2(1), pp. 1-20, 2021.

[35] Y.D. Yolanda, A.B.D. Nandiyanto, "How to read and calculate diameter size from electron microscopy images," *ASEAN Journal of Science and Engineering Education*, vol. 2(1), pp. 11-36, 2022.

[36] B. Buhani, S. Suharso, Z. Sembiring, "Biosorption of metal Ions Pb (II), Cu (II), and Cd (II) on sargassum duplicatum immobilized silica gel matrix," *Indonesian Journal of Chemistry*, vol. 6(3), pp. 245-250, 2006.

[37] N. Ayawei, A. N. Ebelegi, D. Wankasi, "Modelling and interpretation of adsorption isotherms," *Journal of chemistry*, vol. 2017, pp. 1-11, 2017.

[38] A. B. D. Nandiyanto, G. C. S. Girsang, R. Maryanti, R. Ragadhita, S. Anggraeni, F. M. Fauzi, A. S. M. Al-Obaidi, "Isotherm adsorption characteristics of carbon microparticles prepared from pineapple peel waste," *Communications in Science and Technology*, vol. 5(1), pp. 31-39, 2020.

[39] A.B.D. Nandiyanto, S.R. Putri, S. Anggraeni, T. Kurniwan, "Isotherm adsorption OF 3000-μm natural zeolite," *Journal of Engineering Science and Technology*, vol. 17(4), pp. 2447-2460, 2022.

[40] M. Peng, A.V. Nguyen, J. Wang, R. Miller, "A critical review of the model fitting quality and parameter stability of equilibrium adsorption models," *Advances in Colloid and Interface Science*, vol. 262, pp. 50-68, 2018.

[41] J. Liu, X. Wang, "Novel silica-based hybrid adsorbents: lead (II) adsorption isotherms," *The Scientific World Journal*, vol. 2013, pp. 1-6, 2013.

[42]   A. B. D. Nandiyanto, "Isotherm adsorption of carbon microparticles prepared from pumpkin (Cucurbita maxima) seeds using two-parameter monolayer adsorption models and Equations," *Moroccan Journal of Chemistry*, vol. 8(3), pp. 8-3, 2020.

[43]   P. S. Kumar, L. Korving, K. J. Keesman, M. C. van Loosdrecht, G. J. Witkamp, "Effect of pore size distribution and particle size of porous metal oxides on phosphate adsorption capacity and kinetics," *Chemical Engineering Journal*, vol. 358, pp. 160-169, 2019.

[44]   I. N. Najm, V. L. Snoeyink, M. T. Suidan, C. H. Lee, Y. Richard, "Effect of particle size and background natural organics on the adsorption efficiency of PAC," *Journal-American Water Works Association*, vol. 82(1), pp. 65-72, 1990.

[45]   A. B. D. Nandiyanto, W. C. Nugraha, I. Yustia, R. Ragadhita, M. Fiandini, M. Saleh, D. R. Ningwulan, "Rice husk for adsorbing dyes in wastewater: literature review of agricultural waste adsorbent, preparation of Rice husk particles, particle size on adsorption characteristics with mechanism and adsorption isotherm," *Journal of Advanced Research in Applied Mechanics*, vol. 106(1), pp. 1-13, 2023.